Biophysical Journal, Volume *122*

Supplemental information

Rho MultiBinder, a fluorescent biosensor that reports the activity of multiple GTPases

Frederico M. Pimenta, Jaewon Huh, Bryan Guzman, Diepreye Amanah, Daniel J. Marston, Nicholas K. Pinkin, Gaudenz Danuser, and Klaus M. Hahn

Supporting Material

Rho MultiBinder, a fluorescent biosensor that reports the activity of multiple GTPases

Frederico M. Pimenta[1,#,] , Jaewon Huh[2,*], Bryan Guzman[1], Diepreye Amanah[1], Daniel J. Marston[1], Nicholas K. Pinkin[1], Gaudenz Danuser,[2] and Klaus M. Hahn[1,#]*

[1]Department of Pharmacology, University of North Carolina at Chapel Hill, Chapel Hill, NC, USA

[2]Departments of Bioinformatics and Cell Biology, University of Texas Southwestern Medical Center, Dallas, TX, USA

[*]these authors contributed equally

[#]please address correspondence to Klaus M. Hahn at khahn@med.unc.edu.

Running title: Multi-target FRET biosensor

SUPPLEMENTAL TEXT

Text S1: Analysis of GTPase crosstalk in dual and triple imaging experiments

The dual imaging data set consisted of 29 cells with Cdc42 and RhoA, and 20 cells with Rac1 and RhoA, measured on 4 different days under identical experimental conditions. The triple imaging data set consisted of 17 cells measured on 2 days. The cross-correlation levels and protrusion/retraction dynamics were checked for each cell individually before applying statistical analysis to verify that all cells were in a comparable state. After checking the external and internal expression mentioned throughout the paper, the biosensor signals were converted into per-cell Z-scores, normalizing the dynamic range of the fluctuations across cells.

To analyze the signaling hierarchy among the co-observed signals we complemented the cross correlation analysis with a directional analysis, asking how the odds of putative effector activation were increased by the activation of a putative target signal. We consider two signals directionally coupled if the odds for such an increase were above random. The analysis was applied twice per GTPase pair, switching the assignment of effector / target signals. Details of how we identified effector/target interactions and the odds ratio of ensuing target signal activation are provided in the Materials and Methods section.

Text S2: MB engineering rounds

MB, a chimera of PBD and RBD, was generated through 3 sequential optimization rounds (see Table S2).

First round (C1.1-C1.3): PBD and RBD were each split into three broad regions and mixed (Figure 3D, Table S2, C1.1-1.3). Binding to Rac1, RhoA and Cdc42 was examined by measuring FRET efficiency relative to constitutively active GTPases in a high-throughput screening assay (1). This allowed us to identify critical regions for binding RhoA, Rac1 and Cdc42. Specifically, for an extended PBD AR (with 84 a.a.), the first 17 a.a. and last 14 a.a. could be replaced without significant loss of FRET, so long as the highly conserved CRIB domain (ISLPSDFEHTIHVG) (2) was kept unchanged (C1.2 and 1.3). For the RhoA AR, removal of the first 17 and last 23 a.a. of the RBD domain had a small but noticeable effect on binding affinity (C1.1).

Second round (C2.1-C2.4): Further studies showed that the RBD domain retained high FRET efficiency when binding RhoA if the first 10 a.a. (starting *"RQMALSL"*; Figure 3C and Table S2, C2.4) were removed. Extension of

the PBD after and not before the conserved CRIB domain was essential for effective Rac1 and Cdc42 sensing (Figure 3C and Table S2, C2.1 vs C2.4). Modifying the conserved CRIB domain with point mutations to include residues on RBD critical for RhoA binding did not yield an efficient affinity reagent for Rac1, RhoA or Cdc42 (Figure 3C and Table S2, C2.2 and 2.3).

Third round (C3.1-C3.10): Based on the previous rounds, we inserted 7-10 a.a. from PBD into Chimera 2.4, between the conserved CRIB region (ISLPSDFEHTIHVG) and the RBD sequence *"RQMALSL"* (Figure 3C and Table S2, C3.1-C3.5). Binding affinity for Rac1 and Cdc42 gradually increased up to ~85% that of the original binding domains (PBD and CBD respectively), while binding to RhoA remained mostly unaltered (~80% of RBD). Interestingly, removal of the 7 critical a.a. *"RQMALSL"* in RBD yielded an efficient binding domain for Rac1 and Cdc42 without inserting anything between the PBD and RBD portions of this chimera (Figure 3C and Table S2, C3.6). However, this caused a decrease in the affinity for RhoA (~60%). Further attempts to either remove a.a. at the end of the RBD sequence and/or extend shorter versions with insertions between the PBD and RBD portions resulted in either no increase in affinity for RhoA and/or no binding to the other two GTPases (Figure 3C and Table S2, C3.7-3.10). This highlighted the need for the *"RQMALSL"* sequence for efficient RhoA binding and proper folding of the RBD affinity reagent, and that PBD and RBD domains needed to be sufficiently separated to permit proper folding and binding to all three GTPases. We chose C3.5 as our GTPase MultiBinder, a 136 a.a. affinity reagent comprised of a 53 a.a. minimal binding motif for Rac and Cdc42, and 83 a.a. for RhoA, producing binding affinities 80-90% those of the original binding domains.

SUPPLEMENTAL FIGURE CAPTIONS

Figure S1 – Effect of biosensor expression on cell edge dynamics. Mouse Embryonic Fibroblasts (MEFs) imaged during random movement, expressing either Ypet-CAAX (gray, n=11), or the following dual-chain FRET biosensors: Ypet-mScarlet Cdc42 (n=19), mAmetrine-Cdc42 (n=7), Rac1 Ypet-mCherry (n=9), RhoA Ypet-mScarlet (n=17) and RhoA Ypet-mCherry (n=8). Comparison of average frequency **(A and D)**, average velocity **(B and E)** and average duration **(C and F)** of protrusions **(A-C)** and retractions **(D-F)** for the control group (Ypet-CAAX) and biosensors. Dunn's Test, one-way ANOVA non-parametric test (Kruskal-Wallis) used for statistical analysis, n.s. – $p > 0.05$, * - $p < 0.05$, ** - $p < 0.01$.

Figure S2 –Dependency of protrusion, retraction and peak correlation on biosensor expression level. MEFs imaged during random movement, expressing either RhoA Ypet-mScarlet (black) or RhoA Ypet-mCherry (red), with analyzed parameters plotted against the relative expression level (measured as fluorescence intensity of Donor FP (Ypet) normalized for cell area and corrected for differences in illumination intensity and exposure time). The following parameters were analyzed: average protrusion and retraction frequency **(A,B)**, average protrusion and retraction velocity **(C,D)**, average protrusion and retraction duration **(E,F)** and minimum peak correlation **(G)**.

Figure S3 – Computational analysis pipeline for correlation of GTPase activity and edge velocity. (A) Example of cell segmentation in 1.4x1.4 µm widows along the cell edge, in layers at different distances from the edge. Color denotes GTPase activation. **(B)** Map of GTPase activity over time measured for each window in layer 1. **(C)** Map of edge velocity over time measured for each window in layer 1, with scale indicating protrusion or retraction velocity. **(D)** Cross correlation of edge velocity vs. Cdc42 activity for each window in layer 1.

Figure S4 – Correlation of biosensor activity and edge velocity as a function of the time lag between the two, for different biosensors and across different layers. This data was obtained from Mouse Embryonic Fibroblasts imaged during random movement. **(A-B)** Ypet-mScarlet Cdc42 (green, n=19) cross-correlation for layers 1 (0-1.4 µm) and 2 (1.4-2.8 µm). **(C-D)** mAmetrine-mScarlet Cdc42 (blue, n=7). **(E-F)** Ypet-mScarlet RhoA (green, n=17). **(G-H)** Ypet-mCherry RhoA (green, n=9). Error bands are 95% CI, individual cells represented as dashed lines.

Figure S5 – RhoA cross-correlation with edge motion is dependent on cell edge velocity. RhoA data collected in the present experiments were consistent with previous data in MDA-MB 231 cells (3), but inconsistent with previous MEF data (4). To understand the origin of this difference we mapped regions with differing protrusion velocities by analyzing individual windows and grouping them based on peak correlation and SD of velocity. This analysis showed that there were two dominant patterns, one of which was consistent with previous observations of maximal positive correlation at ~t0 and correlated with slower velocities. **(A)** Window segmentation of the cell edge (1.4x1.4 μm), colored by GTPase activation. **(B)** Maps of edge velocity over time measured for each window in layer 1. Solid square highlights windows with velocity < 20 nm/s throughout the duration of the movie and dashed square windows with velocities > 20 nm/s. **(C)** Map of GTPase activity over time measured for each window in layer 1. Same square regions described for (B) represented here. **(D)** Map of the cross-correlation between edge velocity and RhoA activity for each window in layer 1. Note the difference between solid (velocities > 20 nm/s) and dashed (velocities < 20 nm/s) squares. **(E)** Scatterplot shows standard deviation of velocity for each individual window analyzed as a function of peak correlation, showcasing a trend towards positive correlation values with lower velocity standard deviation (SD) (n = 8 cells from two individual sets of experiments). Inset: percentage of windows with negative (red) or positive (green) correlation peak values after selection for windows with velocity SD < 20 nm/s (n = 842 windows), < 15 nm/s (n = 476 windows), < 10 nm/s (n = 143 windows), showing the shift from negative to positive correlation peaks as the edge velocity is reduced. **(F)** Per cell-averaged (dashed lines) population-averaged (solid line) cross correlation between biosensor activity and edge velocity for all windows with positive cross-correlation peak integrated over in n=8 cells.

Figure S6 – Validation of MultiBinder (MB) as an affinity reagent. (A) RhoA activity map in a Mouse Embryonic Fibroblast (MEF) during constitutive migration. The MEF was stably expressing mAmetrine-RhoA and mCherry-MB. Comparison of average frequency **(B and E)**, average velocity **(C and F)** and average duration **(D and G)** of protrusions **(A-C)** and retractions **(D-F)** for MEFs expressing either Ypet-CAAX (gray, n=11), Ypet-RhoA with mCherry-RBD (orange, n=8) Ypet-RhoA with mCherry-MB (green, n=5) and mAmetrine-RhoA with mCherry-MB (blue, n=5). Dunn's Test, one-way ANOVA non-parametric test (Kruskal–Wallis) used for statistical analysis. n.s. - non-significant; * - $p < 0.05$; ** - $p < 0.01$; *** - $p < 0.005$. **(H)** Correlation of edge velocity and biosensor activity signal for MEFs expressing either Ypet-RhoA with mCherry-RBD (orange, n=8) or mAmetrine-RhoA with mCherry-MB (blue, n=5); error bands are 95% CI.

Figure S7 – Multibinder (MB) enables simultaneous imaging of 2 GTPases. (A) Correlation of edge velocity with RhoA (left) and Cdc42 (right) activity in MEFs during random movement, for layers 1 (top) and 2 (bottom) (n=17). Cells were stably expressing Ypet-RhoA, mAmetrine-Cdc42 and mCherry-MB. **(B)** Correlation of edge velocity with RhoA (left) and Rac1 (right) activity in MEFs expressing Ypet-RhoA, mAmetrine-Rac1 and mCherry-MB, in Layers 1 (top) and 2 (bottom) (n=13). Error bands are 95% CI, individual cells represented as dashed lines.

Figure S8 – Correlation of GTPase biosensor activity with edge velocity using data obtained from imaging three biosensors in Mouse Embryonic Fibroblasts during random movement. (A) Layer 1 and **(B)** Layer 2 correlations for Rac1 (blue), RhoA (green) and Cdc42 (red). Error bands are 95% CI, individual cells represented as dashed lines (n=8).

Figure S9 – Assaying cell perturbation by measuring cell edge dynamics of MEFs expressing different biosensor combinations. Comparison of average frequency **(A and D)**, average velocity **(B and E)** and average duration **(C and F)** of protrusions **(A-C)** and retractions **(D-F)** for Ypet-CAAX (grey, negative control, n=11) versus cells expressing the RhoA and Cdc42 sensed with MB (green, n=17), RhoA and Rac1 sensed with MB (blue, n=13), triple sensing of RhoA and Rac1 with MB combined with SNAPsense Cdc42 (red, n=8) and RhoA Ypet-mCherry with RBD biosensor (black, n=8), the latter used as a positive control. Error bars are 95% CI. Non-parametric multiple comparison Kruskal-Wallis test used. n.s. - non-significant; * - $p < 0.05$; ** - $p < 0.01$; *** - $p < 0.005$.

SUPPLEMENTAL FIGURES

Figure S1

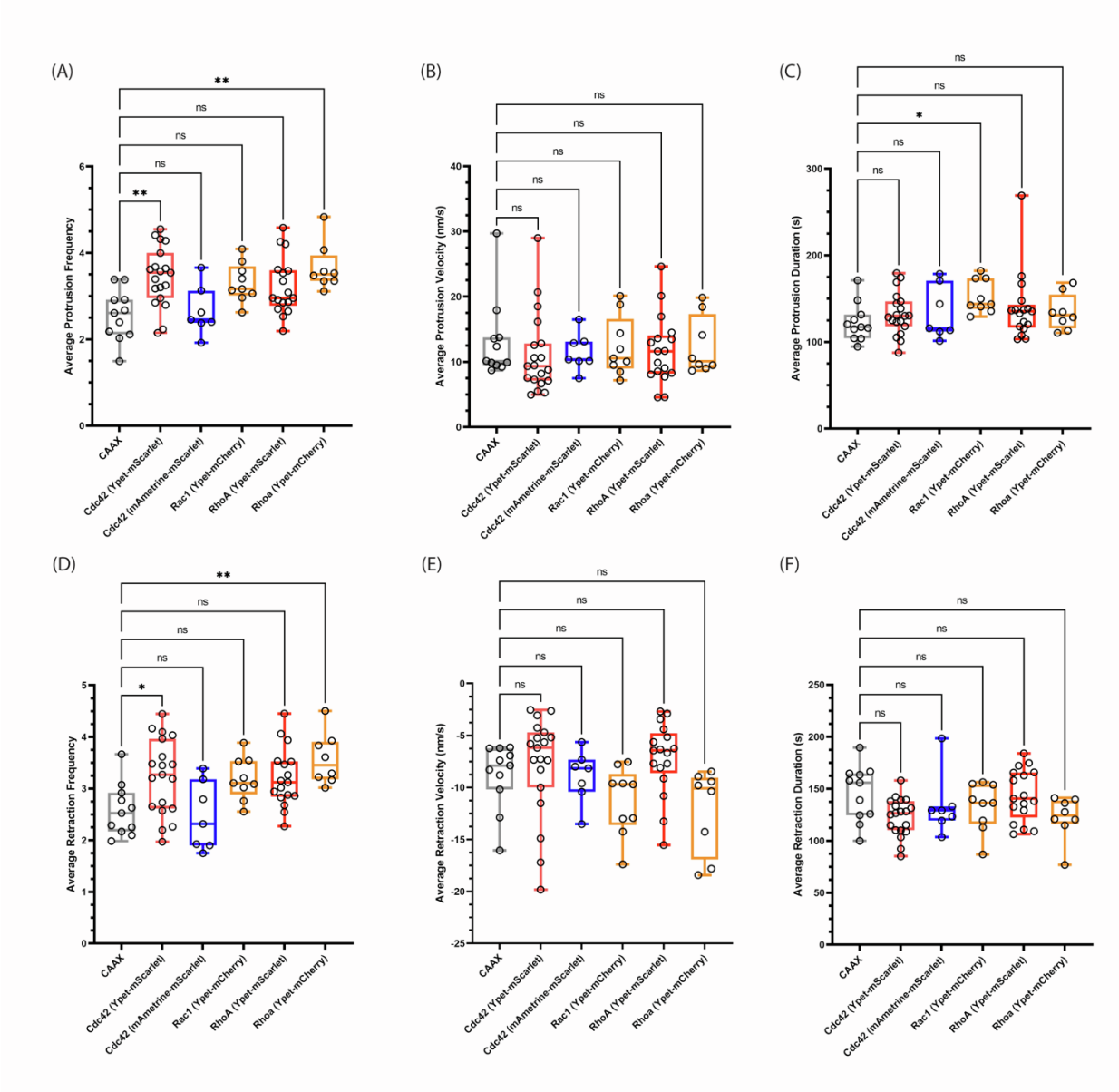

Figure S2

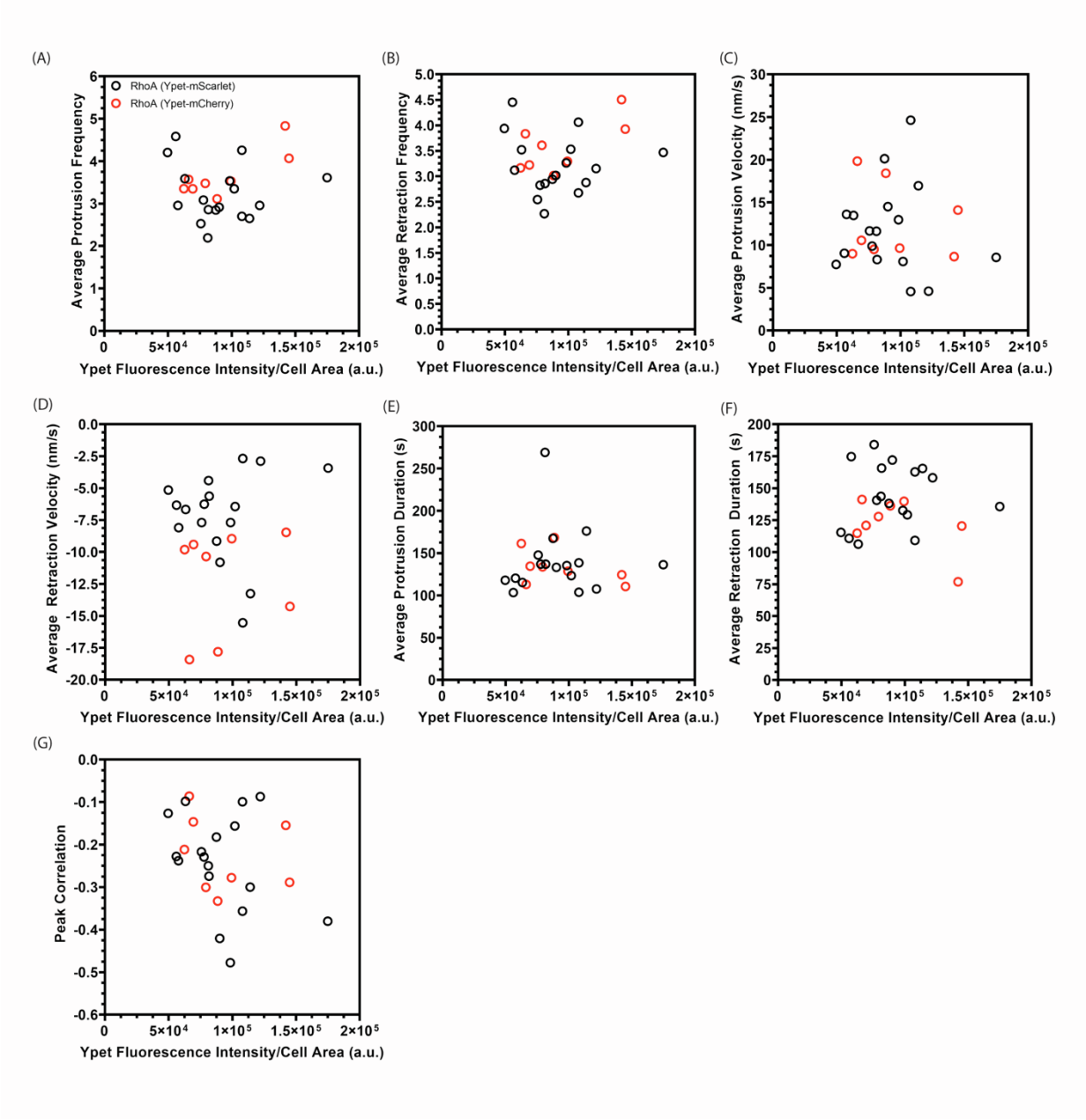
(A)
RhoA (Ypet-mScarlet)
RhoA (Ypet-mCherry)
Average Protrusion Frequency
Ypet Fluorescence Intensity/Cell Area (a.u.)
(B)
Average Retraction Frequency
Ypet Fluorescence Intensity/Cell Area (a.u.)
(C)
Average Protrusion Velocity (nm/s)
Ypet Fluorescence Intensity/Cell Area (a.u.)
(D)
Average Retraction Velocity (nm/s)
Ypet Fluorescence Intensity/Cell Area (a.u.)
(E)
Average Protrusion Duration (s)
Ypet Fluorescence Intensity/Cell Area (a.u.)
(F)
Average Retraction Duration (s)
Ypet Fluorescence Intensity/Cell Area (a.u.)
(G)
Peak Correlation
Ypet Fluorescence Intensity/Cell Area (a.u.)

Figure S3

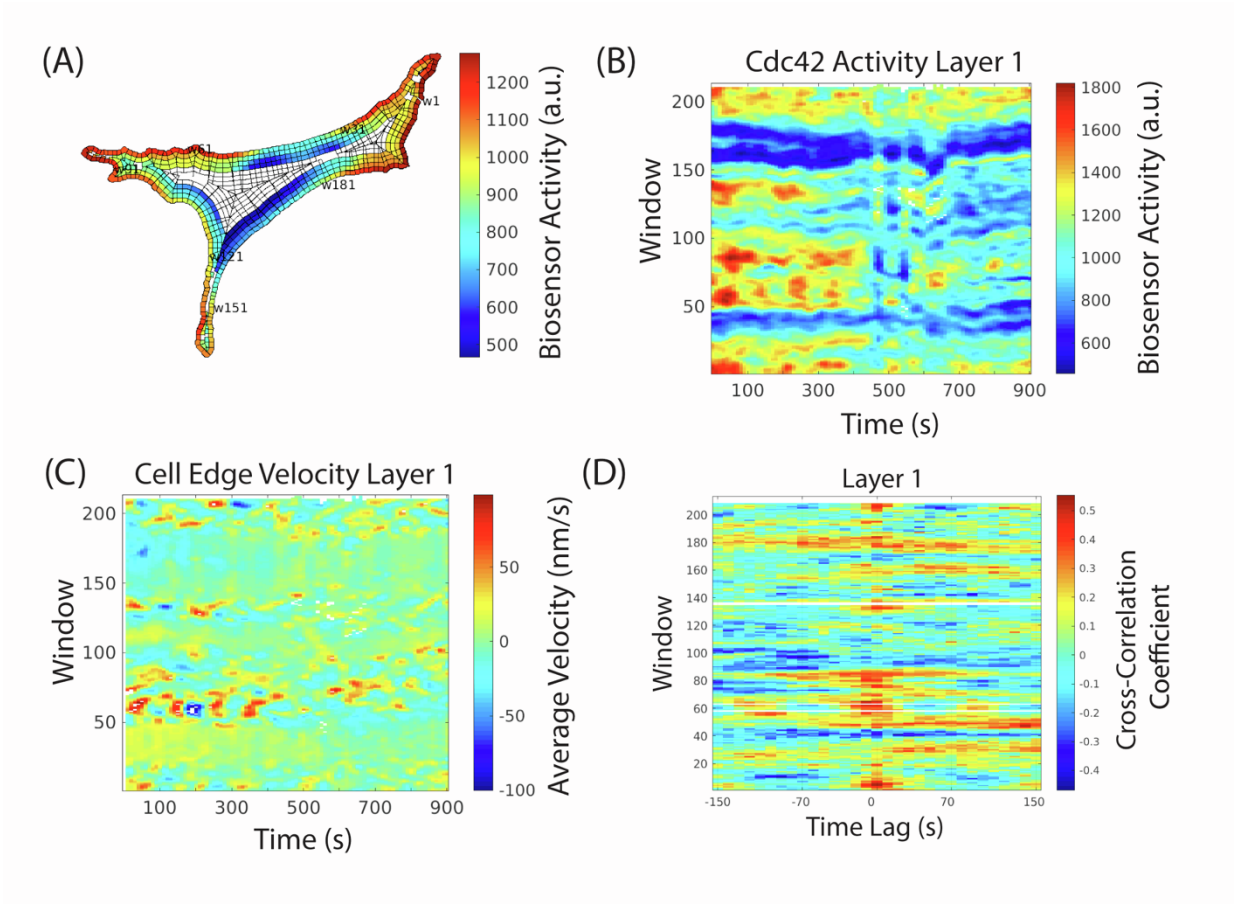
(A)
w1
w61
w121
w181
w241
w301
w151
1200
1100
1000
900
800
700
600
500
Biosensor Activity (a.u.)
(B)
Cdc42 Activity Layer 1
Window
200
150
100
50
100
300
500
700
900
Time (s)
1800
1600
1400
1200
1000
800
600
Biosensor Activity (a.u.)
(C)
Cell Edge Velocity Layer 1
Window
200
150
100
50
100
300
500
700
900
Time (s)
50
0
-50
-100
Average Velocity (nm/s)
(D)
Layer 1
Window
200
180
160
140
120
100
80
60
40
20
-150
-70
0
70
150
Time Lag (s)
0.5
0.4
0.3
0.2
0.1
0
-0.1
-0.2
-0.3
-0.4
Cross-Correlation Coefficient

Figure S4

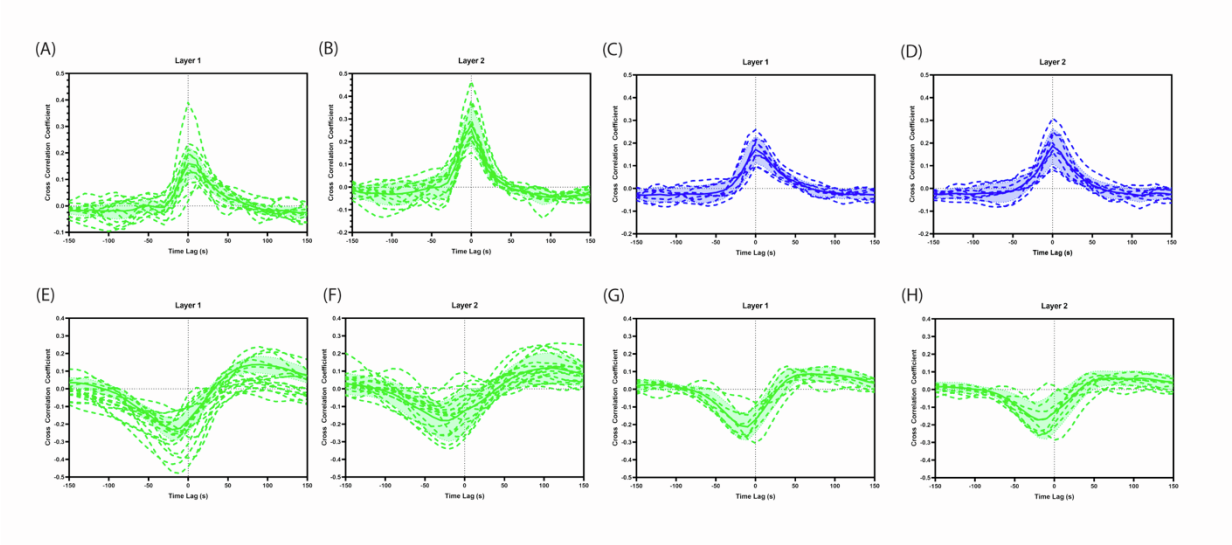
(A)
Layer 1
(B)
Layer 2
(C)
Layer 1
(D)
Layer 2
(E)
Layer 1
(F)
Layer 2
(G)
Layer 1
(H)
Layer 2
Cross Correlation Coefficient
Time Lag (s)

Figure S5

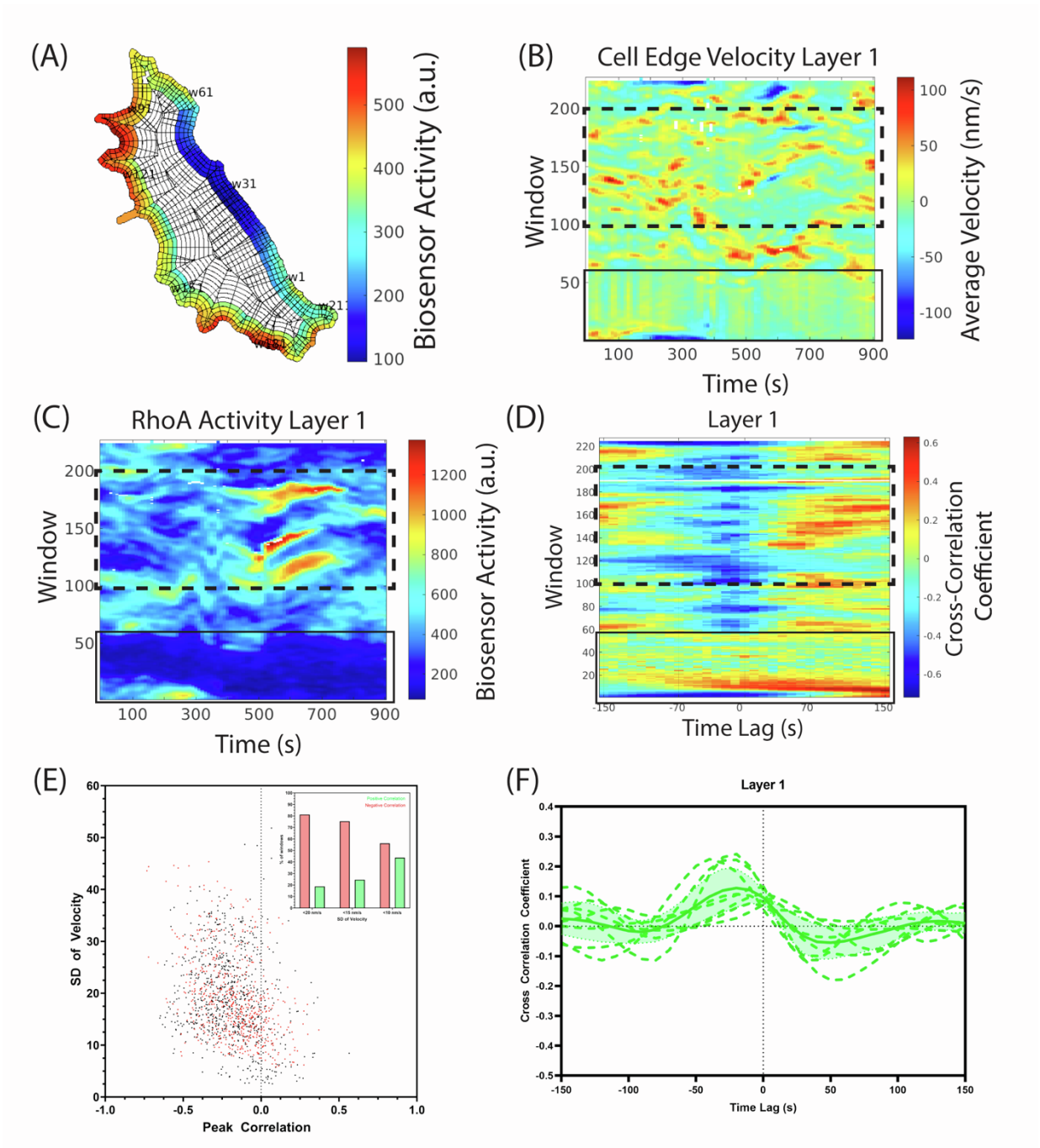
(A)
w61
w31
w1
w121
w181
w241
500
400
300
200
100
Biosensor Activity (a.u.)
(B)
Cell Edge Velocity Layer 1
Window
200
150
100
50
100
300
500
700
900
Time (s)
100
50
0
-50
-100
Average Velocity (nm/s)
(C)
RhoA Activity Layer 1
Window
200
150
100
50
100
300
500
700
900
Time (s)
1200
1000
800
600
400
200
Biosensor Activity (a.u.)
(D)
Layer 1
Window
220
200
180
160
140
120
100
80
60
40
20
-150
-70
0
70
150
Time Lag (s)
0.6
0.4
0.2
0
-0.2
-0.4
-0.6
Cross-Correlation Coefficient
(E)
SD of Velocity
60
50
40
30
20
10
0
-1.0
-0.5
0.0
0.5
1.0
Peak Correlation
(F)
Layer 1
Cross Correlation Coefficient
0.4
0.3
0.2
0.1
0.0
-0.1
-0.2
-0.3
-0.4
-0.5
-150
-100
-50
0
50
100
150
Time Lag (s)

Figure S6

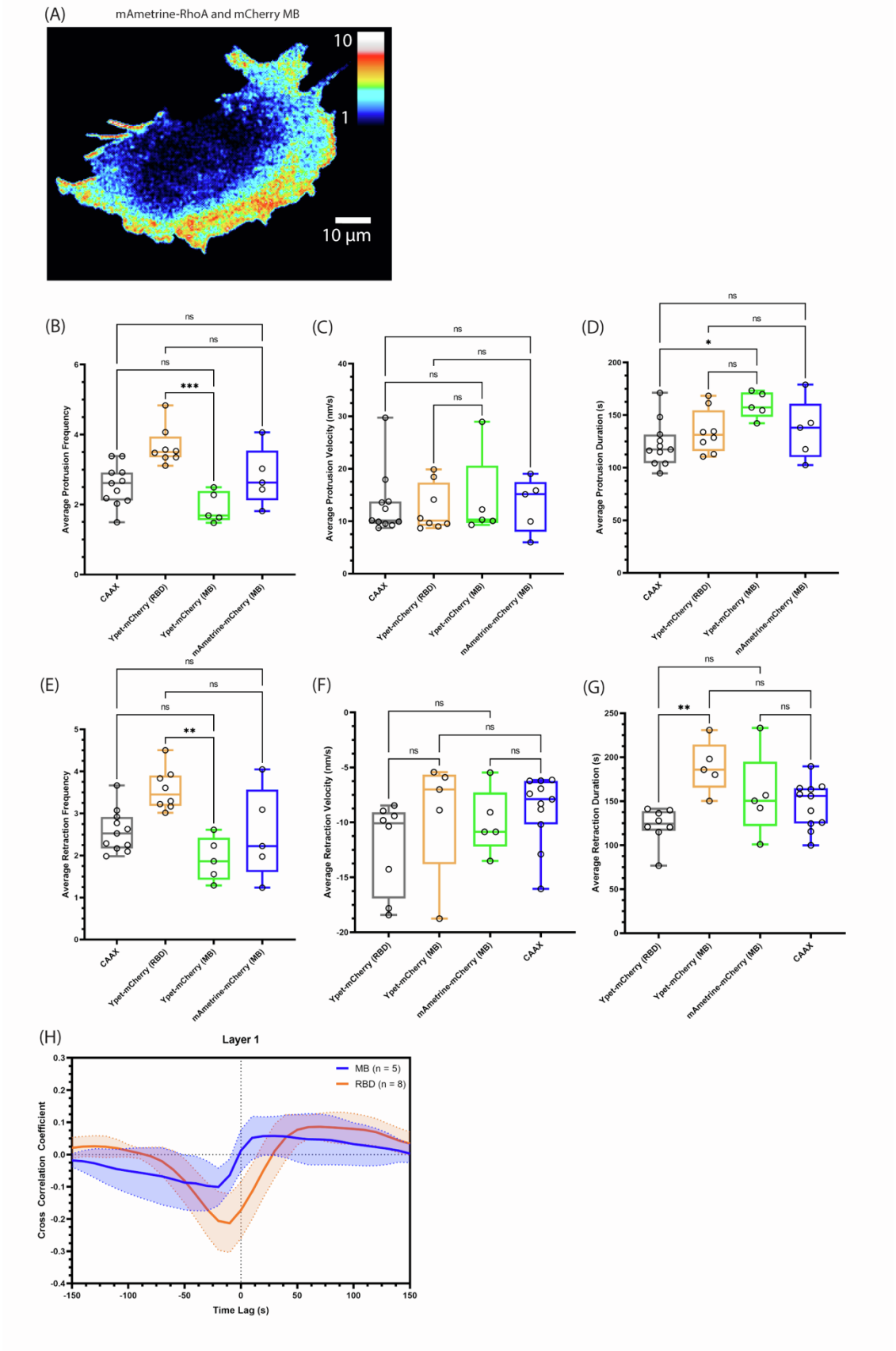
(A)
mAmetrine-RhoA and mCherry MB
10
1
10 µm
(B)
Average Protrusion Frequency
(C)
Average Protrusion Velocity (nm/s)
(D)
Average Protrusion Duration (s)
(E)
Average Retraction Frequency
(F)
Average Retraction Velocity (nm/s)
(G)
Average Retraction Duration (s)
CAAX
Ypet-mCherry (RBD)
Ypet-mCherry (MB)
mAmetrine-mCherry (MB)
ns
*
**
***
(H)
Layer 1
MB (n = 5)
RBD (n = 8)
Cross Correlation Coefficient
Time Lag (s)

Figure S7

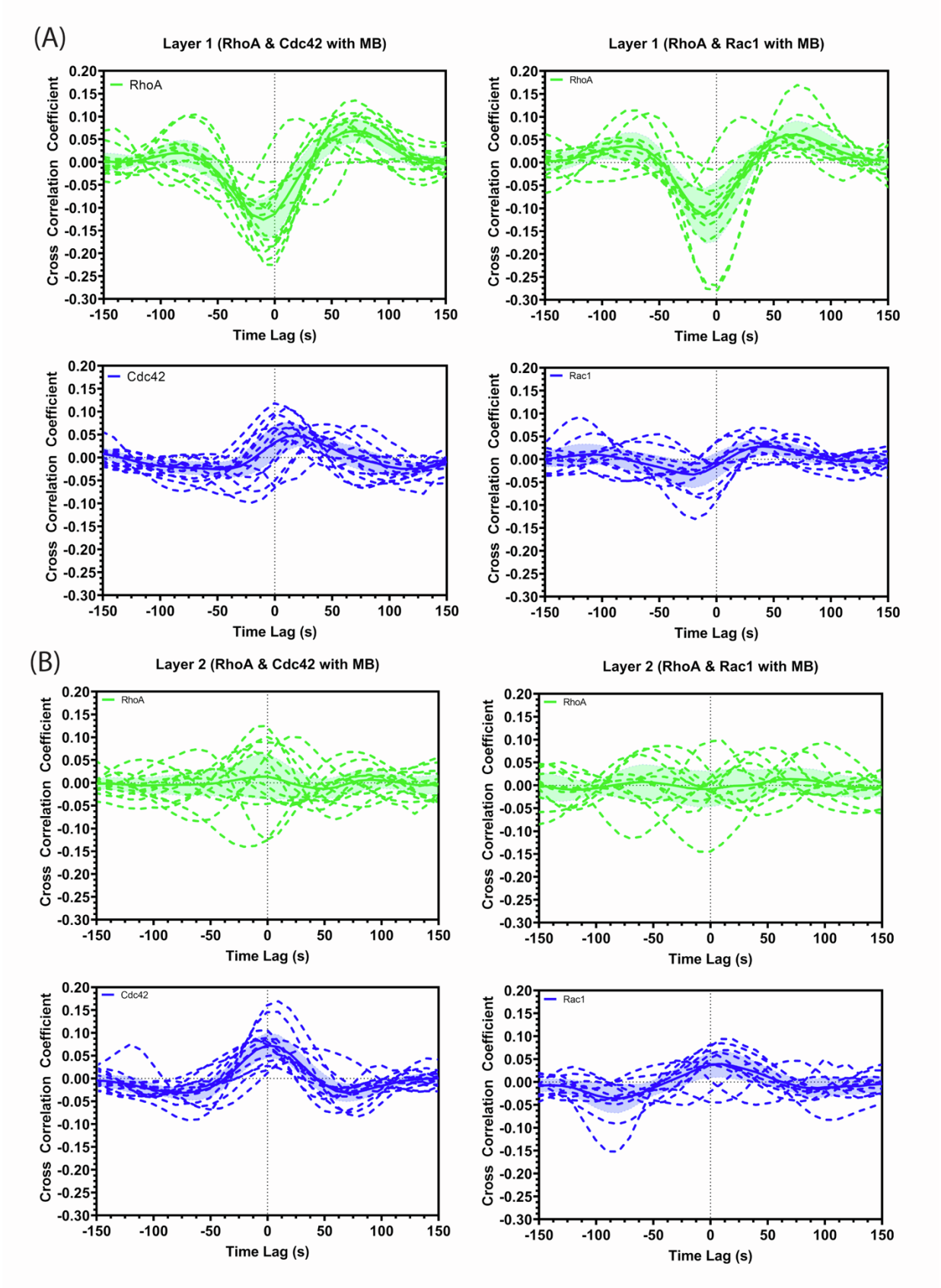
(A)
Layer 1 (RhoA & Cdc42 with MB)
Layer 1 (RhoA & Rac1 with MB)
RhoA
Cdc42
Rac1
Cross Correlation Coefficient
Time Lag (s)
(B)
Layer 2 (RhoA & Cdc42 with MB)
Layer 2 (RhoA & Rac1 with MB)

Figure S8

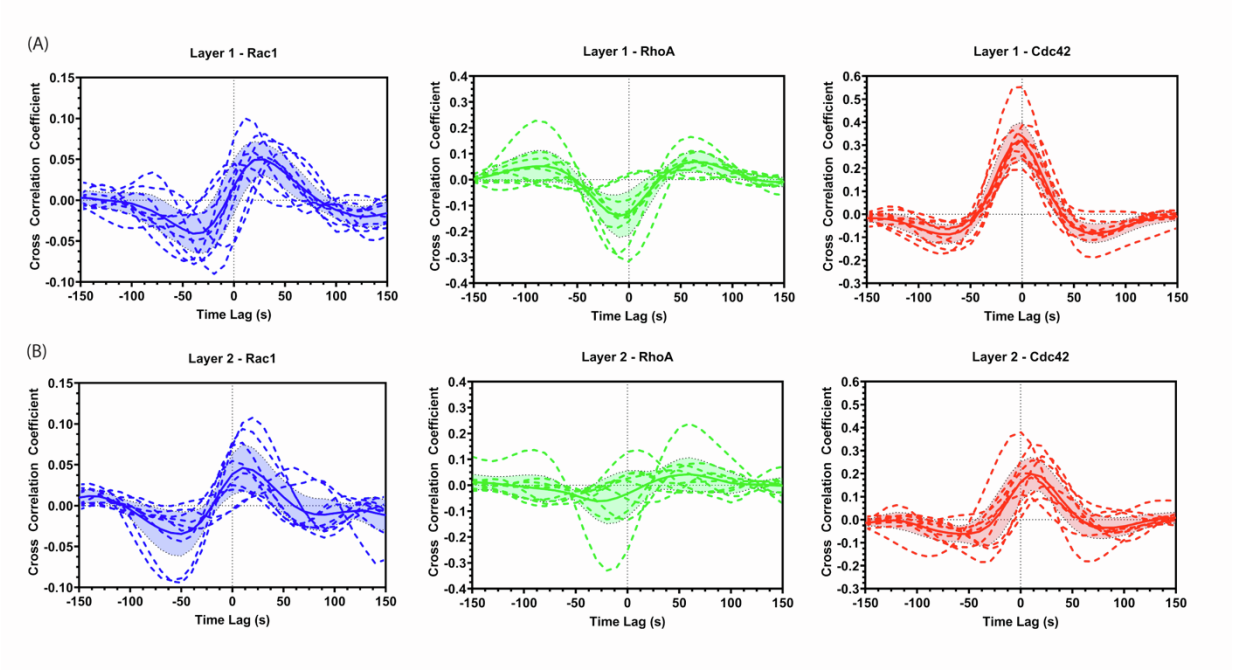
(A)
Layer 1 - Rac1
Layer 1 - RhoA
Layer 1 - Cdc42
(B)
Layer 2 - Rac1
Layer 2 - RhoA
Layer 2 - Cdc42
Cross Correlation Coefficient
Time Lag (s)

Figure S9

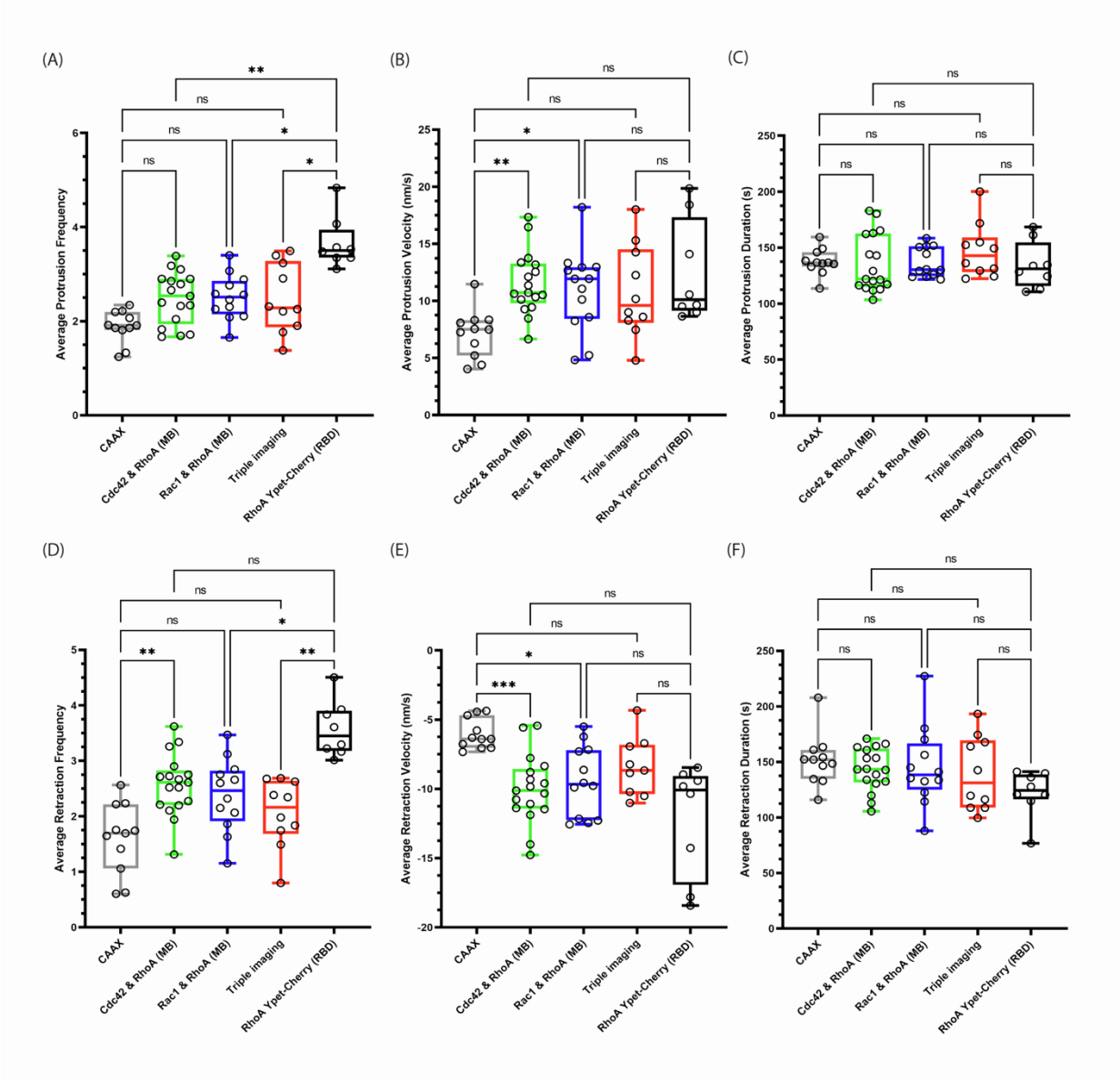
(A)
Average Protrusion Frequency
(B)
Average Protrusion Velocity (nm/s)
(C)
Average Protrusion Duration (s)
(D)
Average Retraction Frequency
(E)
Average Retraction Velocity (nm/s)
(F)
Average Retraction Duration (s)
CAAX
Cdc42 & RhoA (MB)
Rac1 & RhoA (MB)
Triple imaging
RhoA Ypet-Cherry (RBD)
ns
*
**
***

SUPPLEMENTAL TABLES

Table S1. List of new constructs generated in this study, in the manuscript. pB = piggybac.

Name of the construct	Antibiotic Selection
pTriex FLARE dc. 4 His Myc mScarlet-RBD/t2a p2a/Ypet-RhoA CA (Q63L)	Amp
pTriex FLARE dc. 4 His Myc mScarlet-CBD/t2a p2a/Ypet-Cdc42 CA (Q61L)	Amp
pTriex FLARE dc. 4 His Myc mScarlet-PBD90/t2a p2a/Ypet-Rac1 CA (Q61L)	Amp
pTriex FLARE dc. 4 His Myc TagRFP-T-RBD/t2a p2a/Ypet-RhoA CA (Q63L)	Amp
pTriex FLARE dc. 4 His Myc TagRFP-T-CBD/t2a p2a/Ypet-Cdc42 CA (Q61L)	Amp
pTriex FLARE dc. 4 His Myc TagRFP-T-PBD90/t2a p2a/Ypet-Rac1 CA (Q61L)	Amp
pTriex FLARE dc. 4 His Myc mCherry-RBD/t2a p2a/Ypet-RhoA CA (Q63L)	Amp
pTriex FLARE dc. 4 His Myc mCherry-CBD/t2a p2a/Ypet-Cdc42 CA (Q61L)	Amp
pTriex FLARE dc. 4 His Myc mCherry-PBD90/t2a p2a/Ypet-Rac1 CA (Q61L)	Amp
pTriex FLARE dc. 4 His Myc mScarlet-RBD/t2a p2a/cYpet229-RhoA (Q63L)	Amp
pTriex FLARE dc. 4 His Myc mScarlet-RBD/t2a p2a/cYpet173-RhoA (Q63L)	Amp
pTriex FLARE dc. 4 His Myc mScarlet-RBD/t2a p2a/cYpet157-RhoA (Q63L)	Amp
pTriex FLARE dc. 4 His Myc mScarlet-CBD/t2a p2a/cYpet229-Cdc42 (Q61L)	Amp
pTriex FLARE dc. 4 His Myc mScarlet-CBD/t2a p2a/cYpet173-Cdc42 (Q61L)	Amp
pTriex FLARE dc. 4 His Myc mScarlet-CBD/t2a p2a/cYpet157-Cdc42 (Q61L)	Amp
pTriex FLARE dc. 4 His Myc mScarlet-PBD90/t2a p2a/cYpet229-Rac1 CA (Q61L)	Amp
pTriex FLARE dc. 4 His Myc mScarlet-PBD90/t2a p2a/cYpet173-Rac1 CA (Q61L)	Amp
pTriex FLARE dc. 4 His Myc mScarlet-PBD90/t2a p2a/cYpet157-Rac1 CA (Q61L)	Amp
pTriex FLARE dc. 4 His Myc mScarlet-CBD/t2a p2a/Ypet-Cdc42	Amp
pTriex FLARE dc. 4 His Myc mCherry-CBD/t2a p2a/mAmetrine-Cdc42	Amp
pTriex FLARE dc. 4 His Myc mCherry-CBD/t2a p2a/mAmetrine-Cdc42 CA (Q61L)	Amp
pTriex FLARE dc. 4 His Myc mScarlet-RBD/t2a p2a/Ypet-RhoA	Amp
pTriex FLARE dc. 4 His Myc mCherry-RBD/t2a p2a/Ypet-RhoA	Amp
pTriex FLARE dc. 4 His Myc mScarlet-PBD90/t2a p2a/Ypet-Rac1	Amp
pTriex FLARE dc. 4 His Myc mCherry-PBD90/t2a p2a/Ypet-Rac1	Amp
pB mScarlet-CBD/t2a p2a/Ypet-Cdc42	Amp/Hygro
pB mScarlet-CBD/t2a p2a/mAmetrine-Cdc42	Amp/hygro
pB mScarlet-RBD/t2a p2a/Ypet-RhoA	Amp/Higro
pB mCherry-RBD/t2a p2a/Ypet-RhoA	Amp/Blast
pB mCherry-PBD75/t2a p2a/Ypet-Rac1	Amp/Blast
pB Ypet-CAAX	Hygro
pTriex FLARE dc. 4 His Myc mScarlet-Chimera C1.1/t2a p2a/Ypet-Rac1 Q61L (CA)	Amp
pTriex FLARE dc. 4 His Myc mScarlet-Chimera C1.2/t2a p2a/Ypet-Rac1 Q61L (CA)	Amp
pTriex FLARE dc. 4 His Myc mScarlet-Chimera C1.3/t2a p2a/Ypet-Rac1 Q61L (CA)	Amp
pTriex FLARE dc. 4 His Myc mScarlet-Chimera C1.1/t2a p2a/Ypet-RhoA Q63L (CA)	Amp
pTriex FLARE dc. 4 His Myc mScarlet-Chimera C1.2/t2a p2a/Ypet-RhoA Q63L (CA)	Amp
pTriex FLARE dc. 4 His Myc mScarlet-Chimera C1.3/t2a p2a/Ypet-RhoA Q63L (CA)	Amp
pTriex FLARE dc. 4 His Myc mScarlet-Chimera C1.1/t2a p2a/Ypet-Cdc42 Q61L (CA)	Amp
pTriex FLARE dc. 4 His Myc mScarlet-Chimera C1.2/t2a p2a/Ypet-Cdc42 Q61L (CA)	Amp
pTriex FLARE dc. 4 His Myc mScarlet-Chimera C1.3/t2a p2a/Ypet-Cdc42 Q61L (CA)	Amp
pTriex FLARE dc. 4 His Myc mScarlet-Chimera2.1/t2a p2a/Ypet-Rac1 Q61L (CA)	Amp
pTriex FLARE dc. 4 His Myc mScarlet-Chimera2.2/t2a p2a/Ypet-Rac1 Q61L (CA)	Amp
pTriex FLARE dc. 4 His Myc mScarlet-Chimera2.3/t2a p2a/Ypet-Rac1 Q61L (CA)	Amp
pTriex FLARE dc. 4 His Myc mScarlet-Chimera2.4/t2a p2a/Ypet-Rac1 Q61L (CA)	Amp
pTriex FLARE dc. 4 His Myc mScarlet-Chimera2.1/t2a p2a/Ypet-RhoA Q63L (CA)	Amp

pTriex FLARE dc. 4 His Myc mScarlet-Chimera2.2/t2a p2a/Ypet-RhoA Q63L (CA)	Amp
pTriex FLARE dc. 4 His Myc mScarlet-Chimera2.3/t2a p2a/Ypet-RhoA Q63L (CA)	Amp
pTriex FLARE dc. 4 His Myc mScarlet-Chimera2.4/t2a p2a/Ypet-RhoA Q63L (CA)	Amp
pTriex FLARE dc. 4 His Myc mScarlet-Chimera2.1/t2a p2a/Ypet-Cdc42 Q61L (CA)	Amp
pTriex FLARE dc. 4 His Myc mScarlet-Chimera2.2/t2a p2a/Ypet-Cdc42 Q61L (CA)	Amp
pTriex FLARE dc. 4 His Myc mScarlet-Chimera2.3/t2a p2a/Ypet-Cdc42 Q61L (CA)	Amp
pTriex FLARE dc. 4 His Myc mScarlet-Chimera2.4/t2a p2a/Ypet-Cdc42 Q61L (CA)	Amp
pTriex FLARE dc. 4 His Myc mCherry-Chimera3.1/t2a p2a/Ypet-Rac1 Q61L (CA)	Amp
pTriex FLARE dc. 4 His Myc mCherry-Chimera3.2/t2a p2a/Ypet-Rac1 Q61L (CA)	Amp
pTriex FLARE dc. 4 His Myc mCherry-Chimera3.3/t2a p2a/Ypet-Rac1 Q61L (CA)	Amp
pTriex FLARE dc. 4 His Myc mCherry-Chimera3.4/t2a p2a/Ypet-Rac1 Q61L (CA)	Amp
pTriex FLARE dc. 4 His Myc mCherry-Chimera3.6/t2a p2a/Ypet-Rac1 Q61L (CA)	Amp
pTriex FLARE dc. 4 His Myc mCherry-Chimera3.7/t2a p2a/Ypet-Rac1 Q61L (CA)	Amp
pTriex FLARE dc. 4 His Myc mCherry-Chimera3.8/t2a p2a/Ypet-Rac1 Q61L (CA)	Amp
pTriex FLARE dc. 4 His Myc mCherry-Chimera3.9/t2a p2a/Ypet-Rac1 Q61L (CA)	Amp
pTriex FLARE dc. 4 His Myc mCherry-Chimera3.10/t2a p2a/Ypet-Rac1 Q61L (CA)	Amp
pTriex FLARE dc. 4 His Myc mCherry-Chimera3.1/t2a p2a/Ypet-RhoA Q63L (CA)	Amp
pTriex FLARE dc. 4 His Myc mCherry-Chimera3.2/t2a p2a/Ypet-RhoA Q63L (CA)	Amp
pTriex FLARE dc. 4 His Myc mCherry-Chimera3.3/t2a p2a/Ypet-RhoA Q63L (CA)	Amp
pTriex FLARE dc. 4 His Myc mCherry-Chimera3.4/t2a p2a/Ypet-RhoA Q63L (CA)	Amp
pTriex FLARE dc. 4 His Myc mCherry-Chimera3.5/t2a p2a/Ypet-RhoA Q63L (CA)	Amp
pTriex FLARE dc. 4 His Myc mCherry-Chimera3.6/t2a p2a/Ypet-RhoA Q63L (CA)	Amp
pTriex FLARE dc. 4 His Myc mCherry-Chimera3.7/t2a p2a/Ypet-RhoA Q63L (CA)	Amp
pTriex FLARE dc. 4 His Myc mCherry-Chimera3.8/t2a p2a/Ypet-RhoA Q63L (CA)	Amp
pTriex FLARE dc. 4 His Myc mCherry-Chimera3.9/t2a p2a/Ypet-RhoA Q63L (CA)	Amp
pTriex FLARE dc. 4 His Myc mCherry-Chimera3.10/t2a p2a/Ypet-RhoA Q63L (CA)	Amp
pTriex FLARE dc. 4 His Myc mCherry-Chimera3.1/t2a p2a/Ypet-Cdc42 Q61L (CA)	Amp
pTriex FLARE dc. 4 His Myc mCherry-Chimera3.2/t2a p2a/Ypet-Cdc42 Q61L (CA)	Amp
pTriex FLARE dc. 4 His Myc mCherry-Chimera3.3/t2a p2a/Ypet-Cdc42 Q61L (CA)	Amp
pTriex FLARE dc. 4 His Myc mCherry-Chimera3.4/t2a p2a/Ypet-Cdc42 Q61L (CA)	Amp
pTriex FLARE dc. 4 His Myc mCherry-Chimera3.5/t2a p2a/Ypet-Cdc42 Q61L (CA)	Amp
pTriex FLARE dc. 4 His Myc mCherry-Chimera3.6/t2a p2a/Ypet-Cdc42 Q61L (CA)	Amp
pTriex FLARE dc. 4 His Myc mCherry-Chimera3.7/t2a p2a/Ypet-Cdc42 Q61L (CA)	Amp
pTriex FLARE dc. 4 His Myc mCherry-Chimera3.8/t2a p2a/Ypet-Cdc42 Q61L (CA)	Amp
pTriex FLARE dc. 4 His Myc mCherry-Chimera3.9/t2a p2a/Ypet-Cdc42 Q61L (CA)	Amp
pTriex FLARE dc. 4 His Myc mCherry-Chimera3.10/t2a p2a/Ypet-Cdc42 Q61L (CA)	Amp
pTriex FLARE dc. 4 His Myc mCherry-Chimera3.5/t2a p2a/Ypet-Rac1	Amp
pTriex FLARE dc. 4 His Myc mCherry-Chimera3.5/t2a p2a/Ypet-RhoA	Amp
pTriex FLARE dc. 4 His Myc mCherry-Chimera3.5/t2a p2a/Ypet-Cdc42	Amp
pTriex FLARE dc. 4 His Myc mCherry-Chimera3.5/t2a p2a/mAmetrine-Rac1	Amp
pTriex FLARE dc. 4 His Myc mCherry-Chimera3.5/t2a p2a/mAmetrine-RhoA	Amp
pTriex FLARE dc. 4 His Myc mCherry-Chimera3.5/t2a p2a/mAmetrine-Cdc42	Amp
pB mCherry-Chimera3.5/t2a p2a/Ypet-RhoA	Amp/Blast
pB mCherry-Chimera3.5/t2a p2a/mAmetrine-RhoA (blast selection)	Amp/blast
pB mAmetrine-Rac1 (hygro)	Amp/hygro
pB mAmetrine-Cdc42 (hygro)	Amp/hygro
pB-HaloTag-CBD-SNAP-Cdc42	Puro

Table S2 – Primary sequence for described affinity reagents. Conserved CRIB domain region in PBD and critical binding domain in RBD identified in this study are underlined. In chimeric constructs (C1.1-C3.10), PBD and RBD regions are colored red and blue, respectively.

AR	*Primary Sequence*
PBD92	ILPGDKTNKKKEKERPEISLPSDFEHTIHVGFDAVTGEFTGMPEQWARLLQTSNITKSEQKKNPQAVLDVLEFYNSKKTSNSQK
RBD	ILEDLNMLYIRQMALSLEDTELQRKLDHEIRMRDGACKLLAACSQREQALEATKSLLVCNSRILSYMGELQRRKEAQVLEKTGRRPSDSVQPA
C1.1	ILPGDKTNKKKEKERPEIEDTELQRKLDHEIRMRDGACKLLAACSQREQALEATKSLLVCNSRILSYMGELLEFYNSKKTSNSQK
C1.2	ILEDLNMLYIRQMALSLISLPSDFEHTIHVGFDAVTGEFTGMPEQWARLLQTSNITKSEQKKNPQAVLDVQRRKEAQVLEKTGRK
C1.3	ILEDLNMLYIRQMALSLISLPSDFEHTIHVGFDAVTGEFTGMPEQWARLLQTSNITKSEQKKNPQAVLDVLEFYNSKKTSNSQK
C2.1	ILPGDKTNKKKEKERPEIISLPSDFEHTIHVGMRDGACKLLAACSQREQALEATKSLLVCNSRILSYMGELQRRKEAQVLEKTGRRPSDSVQPA
C2.2	ILPGDKTNKKKEKERPEII**TE**P**QR**F**L**H**HE**HVGMRDGACKLLAACSQREQALEATKSLLVCNSRILSYMGELQRRKEAQVLEKTGRRPSDSVQPA
C2.3	ILPGDKTNKKKEKERPEII**TE**P**QRKL**F**L**H**HE**HVGMRDGACKLLAACSQREQALEATKSLLVCNSRILSYMGELQRRKEAQVLEKTGRRPSDSVQPA
C2.4	ISLPSDFEHTIHVGRQMALSLEDTELQRKLDHEIRMRDGACKLLAACSQREQALEATKSLLVCNSRILSYMGELQRRKEAQVLEKTGRRPSDSVQPA
C3.1	ISLPSDFEHTIHVGFDAVTGEFTGRQMALSLEDTELQRKLDHEIRMRDGACKLLAACSQREQALEATKSLLVCNSRILSYMGELQRRKEAQVLEKTGRRPSDSVQPA
C3.2	ISLPSDFEHTIHVGFDAVTGEFTGMPEQWARRQMALSLEDTELQRKLDHEIRMRDGACKLLAACSQREQALEATKSLLVCNSRILSYMGELQRRKEAQVLEKTGRRPSDSVQPA
C3.3	ISLPSDFEHTIHVGFDAVTGEFTGMPEQWARLLQTSNIRQMALSLEDTELQRKLDHEIRMRDGACKLLAACSQREQALEATKSLLVCNSRILSYMGELQRRKEAQVLEKTGRRPSDSVQPA
C3.4	ISLPSDFEHTIHVGFDAVTGEFTGMPEQWARLLQTSNITKSEQKKRQMALSLEDTELQRKLDHEIRMRDGACKLLAACSQREQALEATKSLLVCNSRILSYMGELQRRKEAQVLEKTGRRPSDSVQPA
C3.5	ISLPSDFEHTIHVGFDAVTGEFTGMPEQWARLLQTSNITKSEQKKNPQAVLDVRQMALSLEDTELQRKLDHEIRMRDGACKLLAACSQREQALEATKSLLVCNSRILSYMGELQRRKEAQVLEKTGRRPSDSVQPA
C3.6	ISLPSDFEHTIHVGEDTELQRKLDHEIRMRDGACKLLAACSQREQALEATKSLLVCNSRILSYMGELQRRKEAQVLEKTGRRPSDSVQPA
C3.7	ISLPSDFEHTIHVGRQMALSLEDTELQRKLDHEIRMRDGACKLLAACSQREQALEATKSLLVCNSRILSYMGELQRRKEAQVLEKTGRRP
C3.8	ISLPSDFEHTIHVGRQMALSLEDTELQRKLDHEIRMRDGACKLLAACSQREQALEATKSLLVCNSRILSYMGELQRRKEAQVLE
C3.9	ISLPSDFEHTIHVGFDAVTGEFTGRQMALSLEDTELQRKLDHEIRMRDGACKLLAACSQREQALEATKSLLVCNSRILSYMGELQRRKEAQVLE
C3.10	ISLPSDFEHTIHVGFDAVTGEFTGMPEQWARRQMALSLEDTELQRKLDHEIRMRDGACKLLAACSQREQALEATKSLLVCNSRILSYMGELQRRKEAQVLE

SUPPORTING REFERENCES

1. Slattery, S. D., and K. M. Hahn. 2014. A High-Content Assay for Biosensor Validation and for Examining Stimuli that Affect Biosensor Activity. *Curr Protoc Cell Biol*. 65:14 15 11-31, doi: 10.1002/0471143030.cb1415s65.
2. Burbelo, P. D., D. Drechsel, and A. Hall. 1995. A conserved binding motif defines numerous candidate target proteins for both Cdc42 and Rac GTPases. *J Biol Chem*. 270(49):29071-29074, doi: 10.1074/jbc.270.49.29071.
3. Marston, D. J., M. Vilela, J. Huh, J. Ren, M. L. Azoitei, G. Glekas, G. Danuser, J. Sondek, and K. M. Hahn. 2020. Multiplexed GTPase and GEF biosensor imaging enables network connectivity analysis. *Nat Chem Biol*. 16(8):826-833, doi: 10.1038/s41589-020-0542-9.
4. Machacek, M., L. Hodgson, C. Welch, H. Elliott, O. Pertz, P. Nalbant, A. Abell, G. L. Johnson, K. M. Hahn, and G. Danuser. 2009. Coordination of Rho GTPase activities during cell protrusion. *Nature*. 461(7260):99-103, doi: 10.1038/nature08242.

SUPPLEMENTAL MOVIES

Movie S1 – Mouse Embryonic Fibroblast randomly moving on fibronectin, stably expressing the Ypet-mScarlet Cdc42 dual chain FRET biosensor.

Movie S2 – Mouse Embryonic Fibroblast undergoing polarized migration on fibronectin, with activation at the leading edge. The cell is stably expressing the mAmetrine-mScarlet Cdc42 dual chain FRET biosensor.

Movie S3 – Mouse Embryonic Fibroblast randomly moving on fibronectin, stably expressing the Ypet-mScarlet RhoA dual chain FRET biosensor.

Movie S4 – Mouse Embryonic Fibroblast randomly moving on fibronectin, stably expressing the Ypet-mCherry RhoA dual chain FRET biosensor.

Movie S5 – Mouse Embryonic Fibroblast randomly moving on fibronectin, stably expressing Ypet-RhoA and mCherry-MB.

Movie S6 – Imaging two GTPase activities simultaneously: Mouse Embryonic Fibroblast on fibronectin, stably expressing Ypet-RhoA, mAmetrine-Cdc42 and Multibinder-mCherry.

Movie S7 – Imaging three GTPase activities simultaneously: Mouse Embryonic Fibroblast on fibronectin, stably expressing Ypet-RhoA, mAmetrine-Rac1, Multibinder-mCherry and the SNAPsense dye-based Cdc42 biosensor.